SCIENTIFIC INSTRUMENTATION

Development of instrumental device to measure the Solar irradiance

FINAL DELIVERY

DF0820 - Scientific instrumentation

STUDENT:

Felipe Mendoza Giraldo

fmendozag@eafit.edu.co

PROFFESORS:

Alejandro Marulanda Tobón

Álvaro Velasquez Torres

24/08/2022

Contents

List of Figures

List of Tables

1 Introduction

In the present document, the final results obtained from the scientific instrumentation project will be exposed. First the development of the acquisition program and the programming of the embedded systems will be shown, then the calibration curve of the instrument, and finally the conclusions and future work.

2 Content

2.1 Objectives

In this subsection, the general objective and the specific objectives of the project will be presented.

2.1.1 General Objective

To develop an instrumental device to measure the solar irradiance based in a solar cell generation to predict and optimize the generation of a photovoltaic system.

2.1.2 Specific Objectives

- To design the instrument folowing the Ulrich methodology.
- To design the electronic of the system to design and obtain the measure of the solar irradiance.

- To develop a mathematical model for the solar cells based in the literature to simulate the system.
- To develop and calibrate the instrument.
- To evaluate the performance of the instrument when it is installed in a photo-voltaic system measuring the solar irradiance and determining the generated power of the system.

2.2 Types of solar cells

The silicon-based sensors to estimate the solar irradiation are based on photo-voltaic cells. For this reason along this section the different types of silicon-based solar cells will be explored to determine what is the better type of cells to implement in the instrument. Following, a brief introduction of the different type of silicon-based solar cells will be shown [7]:

- **Amorphous Silicon Solar Cell (A-Si)**: This type of cells are formed by amorphous silicon(A-Si), being this the non-crystalline form of the silicon. A-Si cells are fabricated by plasma-enhanced chemical vapor deposition process which consist of deposit a thin layer of the silicon material (1μm thick) over the substract material (glass, metal or plastic). The structure of the cell is composed by a single sequence of p-i-n layers as shown in Figure 1. Its main advantage is their lower manufacturing cost, their flexibility and lightweight, and its disadvantages are that the single layer cells suffer from degradation in their power output (Range off 15-35%) when they are exposed to the sun. This mechanism of degradation is called the Staebler-Wronski Effect [6, 7].

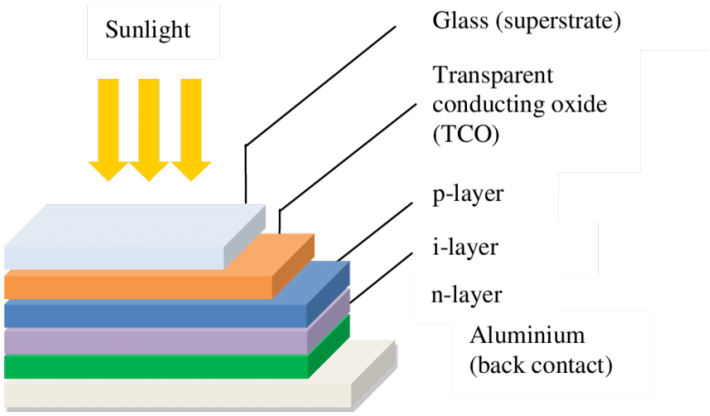

Figure 1: Amorphous silicon solar cells structure, taken from [1]

- **Micromorph Cells (Tandem-Cell Using a-Si/c-Si)**: The micromorph cells are thin film solar cells composed by a multijunction–architecture consisting of two solar cells that are stacked

on top of each other. Thin amorphous silicon top cell absorbs the blue light and the thicker micro-crystalline silicon bottom cell absorbs the red and near-infrared light. In this way this cell cover a wider range of the solar spectrum. The bandgaps of amorphous Silicon (1.7eV) and microcrystalline Silicon (1.1eV) are well suited for this type of solar cells, for this reason the Shockley-Queisser limit of this cell allows conversion efficiencies of over 30% [7]. In figure 2 is presented the structure of this type of solar cells.

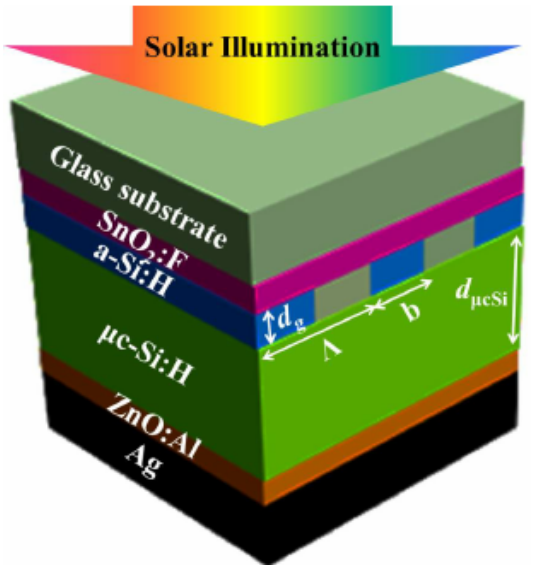

Figure 2: Tandem cells using a-Si/c-Si structure, taken from [2]

- **Monocrystalline Solar Cell (Mono-Si)**: Monocrystalline silicon (Mono-Si) is the base material for silicon chips used in virtually all electronic equipment today. Mono-Si also is utilized for photovoltaic generation as light-absorbing material for the manufacture of solar cells. It consists of silicon in which the crystal lattice of the entire solid is continuous, unbroken to its edges, and free of any grain boundaries. Most silicon mono-crystals are made by the Czochralski process into ingots of up to 2 meters in length and weighing several hundred kilogram's. These cylinders are then sliced into thin wafers of a few hundred microns for further processing [7]. Crystalline panels compared to amorphous panels are typically heavier and more rigid. This type of panels need to be as perpendicular to the sun as possible in order to maintain a high degree of performance and do not tolerate partial shade as well as amorphous solar panels[6]. In Figure 3 is presented the structure of the Mono-Si cells.

- **Polycrystalline Solar Cell (Multi-Si)**: Polycrystalline silicon (Poly-Si) is a high purity, polycrystalline form of silicon, used as a raw material by the solar photovoltaic and electronics industry. As the name suggest, that main different with the monocrystalline cells is that this type of cells

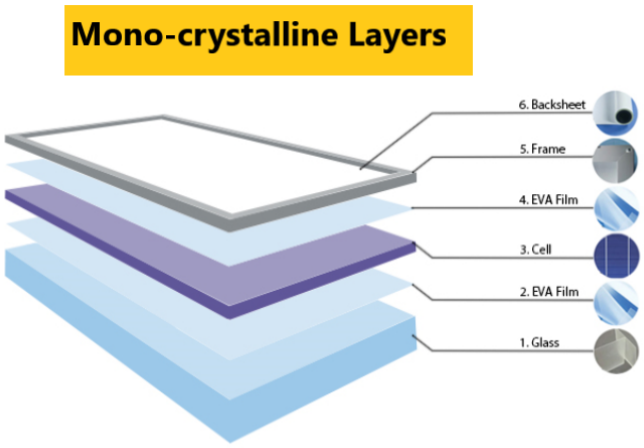

Figure 3: Monocrystalline solar cells structure, taken from [3]

are composed by smaller silicon crystals, also known as crystallites, that give the material its typical metal flake effect. For this reason, this type of cells have lower efficiency than monocrystalline ones but are much cheaper to produce and are the most budget-friendly of the traditional crystalline solar panels. Poly-Si is produced from metallurgical grade silicon by a chemical purification process, called Siemens process by which volatile silicon compounds are distilled down into a more stable form of silicon at high temperatures. In figure 4 is shown how the monocrystalline and the pollycristalline cells looks like. The structure of this type of panels is similar to the monocrystallines ones as shown in Figure 3.

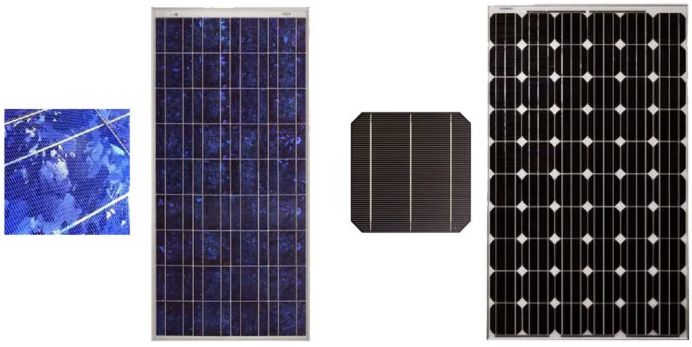

Figure 4: Pollycrystalline and monocrystalline cells comparison, taken from [4]

- **Black Silicon Solar Cells**: Black silicon solar cells are similar to crystalline silicon solar cells. The difference is that black silicon solar cells are treated so that they appear to be black on the surface. The black color tends to absorb more sunlight and in this way this can improve the effiency of the solar cells. The manufacturing process is by adding a dense network of

nanoscale needles on the top of a standar piece of silicon. The black color is also less reflective, so this allow the solar cell to trap light coming from very low angles. The main issue of black silicon cells is something known as carrier recombination. When a photon hits a silicon atom inside a solar cell, the excess energy frees up an electron that is later used to generate electricity [7].

Based on the different types of silicon solar cells explored, a search in the market is carried out to establish which of these cells are available on the market. In this way, in Table 1 a comparison between the more commercial cells.

Table 1: Comparison table of the cells available in the market [6]

	A-Si	**Mono-Si**	**Polly-Si**
Efficiency (%)	7-21	16-28	15-18
Weight	Low	High	High
Strength	Low	High	High
Shade Tolerance	High	Low	Low
Cost ($/W)	0.45-0.53	1.0-1.4	0.80-0.90

Finally, based on Table 1 and the information of the cells presented above the Amorphous Silicon Solar cell is selected for the development of the instrument for the next reasons:

- Is the cell with the lowest price in the market.
- Even if it could be more inefficient than the crystalline cells, as the application doesn't imply power generation, this is not a disadvantage.
- For the internal structure of this type of cell, they are more flexible.

The selected panel is presented in Figure 5. This panel is an Amorphous Silicon panel, and for this reason is flexible, feature that will be used to expand the range of sunlight absorption during all day. The power of the panel is 0.3 [W] and the open source voltage is 2 [V]. Now, to simulate the performance of the cell and to develop the acquisition circuit, a mathematical model for Solar cells will be developed. In the next section the model will be explained deeply.

2.3 Solar cell mathematical model

Modeling a PV cell involves the approximation of the non-linear (I-V) curves. A circuit based model for the solar cells used by many researchers consist of variable current source connected in parallel

Figure 5: Selected panel

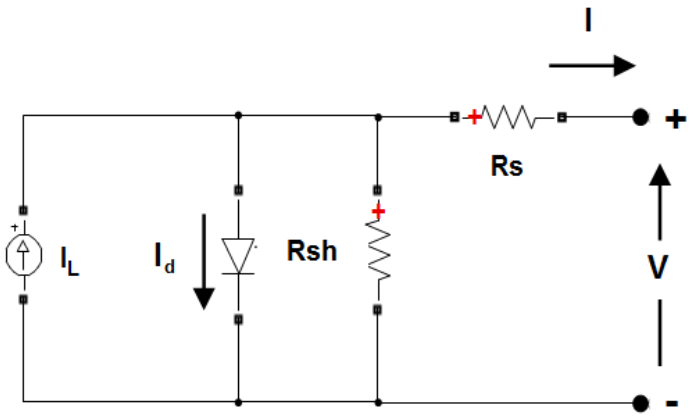

Figure 6: PV cell circuit based model, taken from [5]

to a diode and a resistance known as shunt resistance, and to a series resistance as shown in Figure 6 [8].

Based on Figure 6 and applying the Kirchhoff's circuit laws, the equation 1 is obtained [8]:

$$I = I_L - I_d - I_{Rsh} \tag{1}$$

Being I the output current of the cell, I_L the current source known as the light generated current source, I_d the current of the diode and I_{Rsh} the current in the shunt resistance. The light generated current source I_L is described as the equation 2:

$$I_L = [I_{scr} + K_I(T_c + T_{ref})] \frac{G}{G_{ref}} \tag{2}$$

I_L depends on the solar cell short-circuit current I_{scr}, the cell's short-circuit current temperature coefficient solar insulation K_I, The cell's working and reference temperature T_c and T_{ref} and the solar insulation and reference G and G_{ref}. The diode current I_d is an exponential function as shown in equation 3:

$$I_d = I_s \left[exp\left(\frac{V + IR_s}{nV_T} \right) - 1 \right] \tag{3}$$

Where I_s is the cell saturation of dark current and is obtained from the equation 4, n is the ideality factor, V is the output voltage, R_s is the series resistance of the model and V_T is the thermal voltage described by the equation 6:

$$I_s = I_{RS}\left(\frac{T_c}{T_{ref}}\right)^3 exp\left[\frac{qE_g}{nk}\left(\frac{1}{T_{ref}} - \frac{1}{T_c}\right)\right] \tag{4}$$

$$I_{RS} = \frac{I_{scr}}{exp\left(\frac{qV_{oc}}{nkT_c}\right)} \tag{5}$$

$$V_T = \frac{kT_c}{q} \tag{6}$$

Where I_{RS} is the reverse saturation current at a reference temperature and is estimated with equation 5 shown above, E_g is the band-gap energy and for the Silicon cells this value is 1.10 $[eV]$, k is the Boltzmann's constant ($k = 1.38e-23[J/K]$) and q is the electron charge ($q = 1.6e-19[C]$). Finally the I_{Rsh} is obtained with the equation 7:

$$I_{Rsh} = \frac{V + IR_s}{R_s h} \tag{7}$$

Substituting equations 2, 3, 6 and 7 in 1 the final expression of the model is described in equation 8:

$$I = [I_{scr} + K_I(T_c + T_{ref})]\frac{G}{G_{ref}} - I_s\left[exp\left(\frac{q(V + IR_s)}{nkT_c}\right) - 1\right] - \left[\frac{V + IR_s}{R_s h}\right] \tag{8}$$

All this equations are implemented in Matlab, and the circuit is implemented in Simulink as shown in Figure 7.

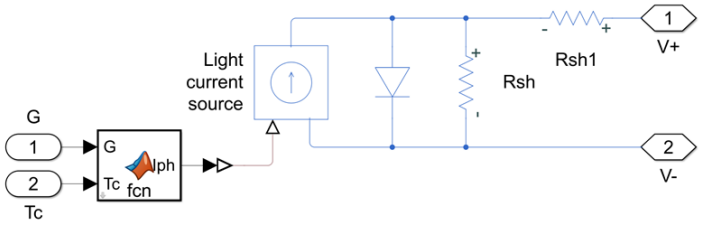

Figure 7: PV model developed in Simulink

This model is applied with the specific panel selected. In table 2 are presented all the parameters for the model implementation for the solar cell selected. Based on the parameters, the I-V curves for the selected solar cell are obtained as shown in Figure 8.

2.4 Calibration curve

To obtain the final calibration curve of the instrument, many measurements of the IV curve of the panel were taken with the experimental setup shown in Figure **??**. In this way, the measure of the

Table 2: Parameters for the model development

Parameter	Value	Units
q	1,6e-19	$[C]$
k	1,38e-23	$[J/K]$
I_{scr}	220	$[mA]$
V_{oc}	2	$[V]$
n	1,1	-
T_{ref}	298,15	$[K]$
G_{ref}	1000	$[W/m^2]$
E_g	1,10	$[eV]$
K_I	1,7e-3	-
R_s	1e-2	$[\Omega]$
R_{sh}	300	$[\Omega]$

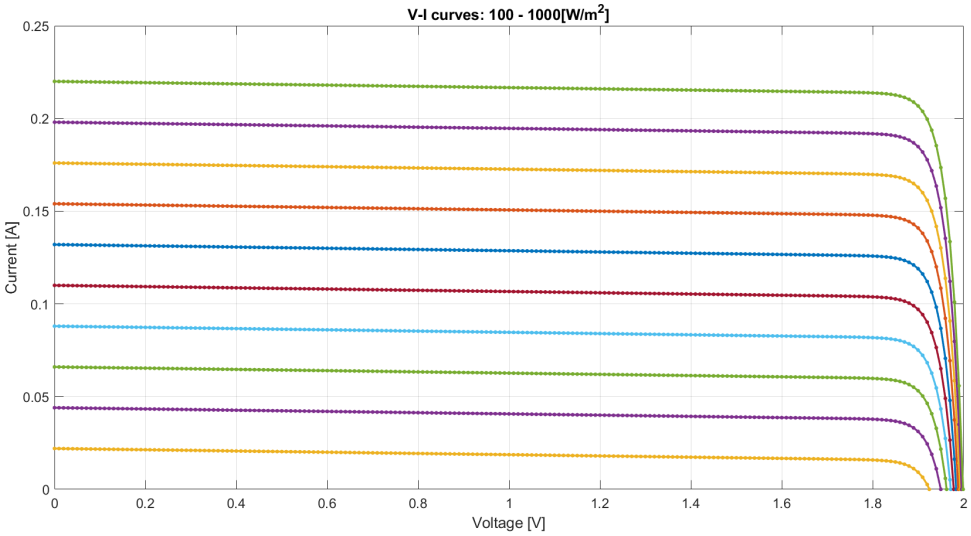

Figure 8: Solar cell VI curves from 100 to 1000 $[W/m^2]$

actual solar irradiance was taken from the calibrated pyranometer, and with the instrumented the VI and the power curves of the panel were obtained. In figures 10 and 11 are presented the curves of the measures taken with the instrument

To estimate the solar irradiance, the areas under the curve were taken from the trapezoidal numerical method to calculate the integration as presented below:

$$P_T = \int_0^{V_{oc}} i(v)dv \tag{9}$$

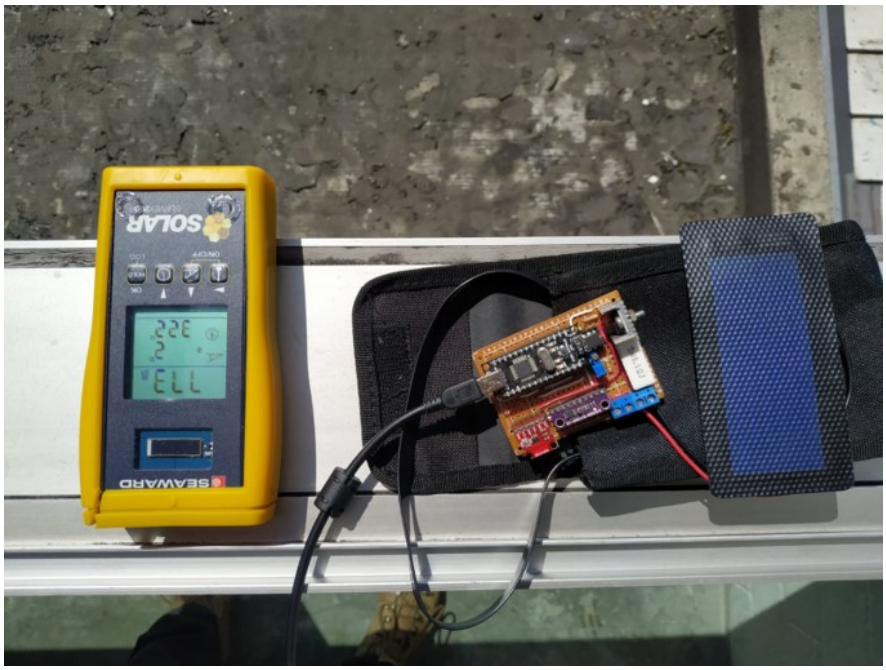

Figure 9: Experimental setup

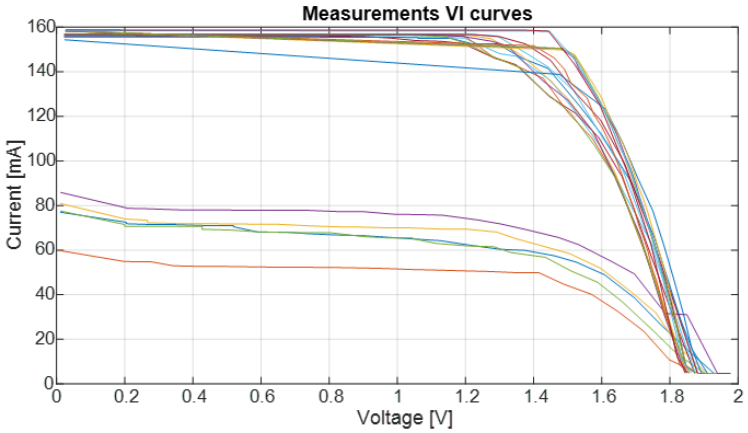

Figure 10: VI measured curves

$$P_T = \sum_{j=0}^{N-1} \frac{(v[j+1] - v[j])(i[j] + i[j+1])}{2} \tag{10}$$

Next, from the measured curves and with the total area under the curve, the calibration curve of the instrument was obtained as shown in Figure 12.

Finally, from the calibration curve, the calibration equation was obtained as shown in the equation below:

$$G(P_T) = 2.223e3[1/m^2]P_T + 248.07[W/m^2] \tag{11}$$

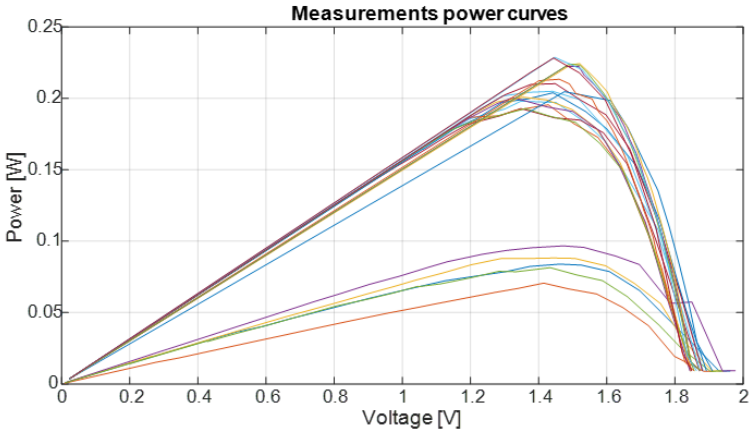

Figure 11: Power measured curves

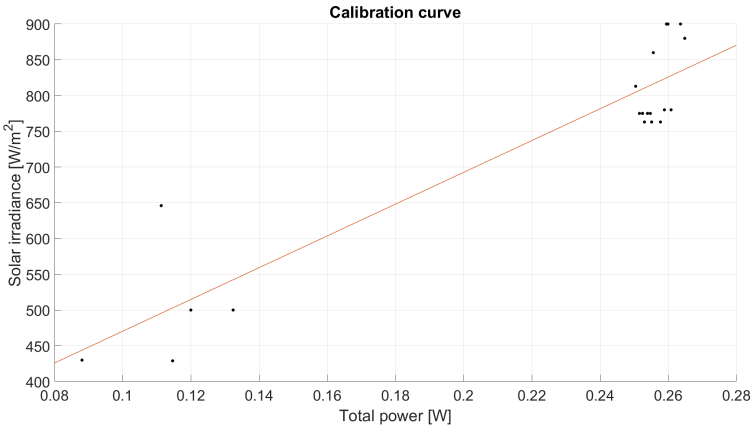

Figure 12: Calibration curve of the instrument.

Where P_T is the total area under the curve VI obtained from the instrument. The r^2 value of the curve obtained is 0.8437.

2.5 Acquisition circuit development

For the development of the acquisition circuit, the block diagram of the circuit is presented in Figure 13 it is started from the shunt resistor, then a first gain stage is implemented to amplify the voltage measurement of the shunt resistor, next a filter is implemented to reduce the noise of the system, then a second gain stage is implemented to adjust the signal to the voltage level of the acquisition system and finally the signal is carried to the system. The shunt resistor has a value of 0.1 Ω, so the voltage of the shunt at the maximum current (0.22A) is:

$$V = 0.1 * 0.22 = 22mV$$

Figure 13: Acquisition circuit block diagram

In the first gain stage, the voltage is adjusted to 500 mV, a non-inverter amplifier configuration is implemented for the gain circuit, so the gain $G1$ is:

$$G1 = 500/22 = 22.7$$

$$G1 = 1 + R2/R1 \longrightarrow R1 = 1K\Omega \longrightarrow R2 = (22.7 - 1) * 1k\Omega = 21.7k\Omega \approx 22k\Omega$$

Then the filter is a passive low-pass filter calculated at a cut frequency of 50Hz to avoid the GRID noise.

$$f_c = 1/(2\pi R3C) \longrightarrow C = 0.1\mu F \longrightarrow R3 = 1/(2\pi 0.1e - 6 * 50) = 32k\Omega \approx 33k\Omega$$

Finally the last gain stage is to elevate the voltage to 5V level. also a non-inverter amplifier configuration is implemented and for the gain circuit, the gain $G2$ is:

$$G2 = 5/0.5 = 10$$

$$G2 = 1 + R5/R4 \longrightarrow R4 = 1K\Omega \longrightarrow R2 = (10 - 1) * 1k\Omega = 9k\Omega \approx 9.1k\Omega$$

The final acquisition circuit is shown in Figure 14 The circuit schematic and the PCB for the instrument

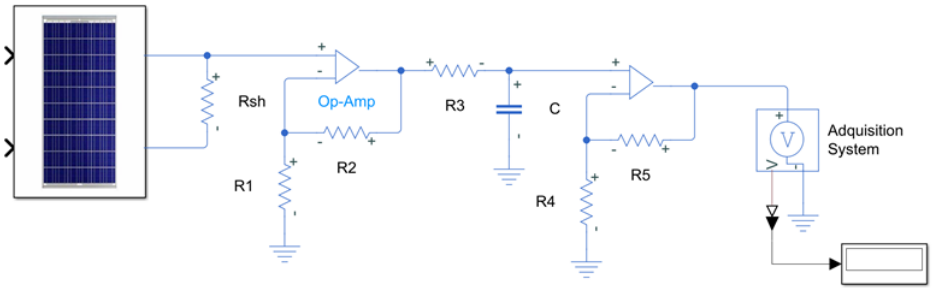

Figure 14: Acquisition circuit

are developed as shown in Figures 15 and 16

Finally, the developed circuit is presented in Figure 17.

2.6 Micro-controller programming

To the circuit, a MOSFET transistor is included in order to control when to enable the short circuit to the cell for reading the current in the instrument. This MOSFET is controlled by the micro-controller.

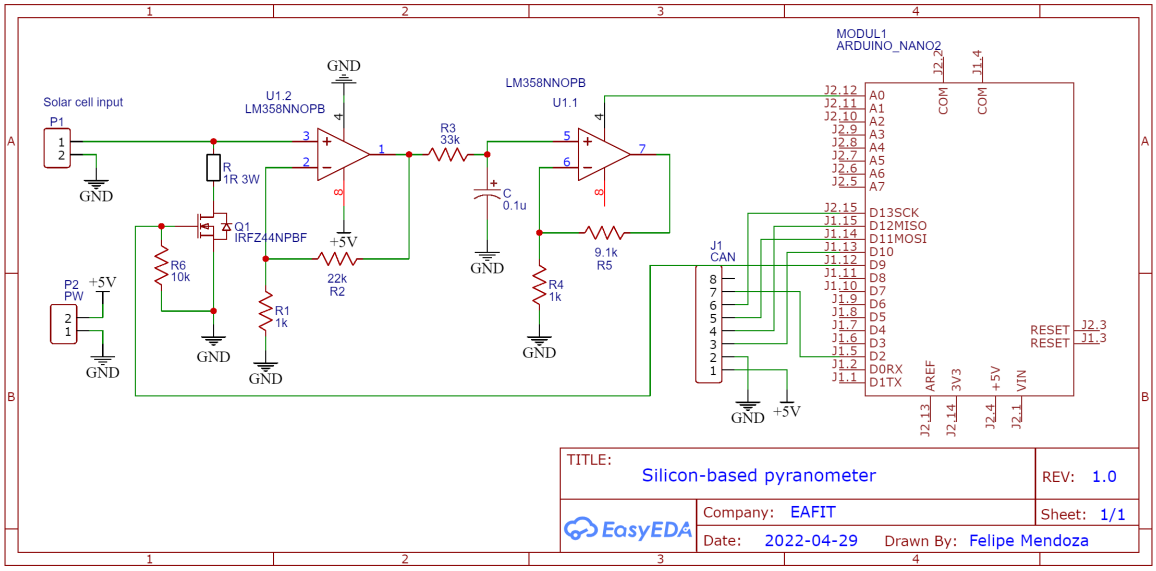

Figure 15: Schematic of the instrument circuit

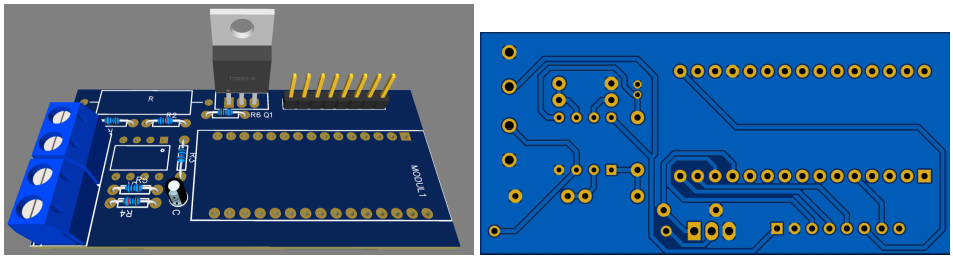

Figure 16: 3D and bottom layer of the PCB

In the present subsection the software of the micro-controller will be explained. In Figure 18 is shown the flow chart of the steps that follow the micro-controller each sample time.

To measure the VI curve, first the program obtain the current or the voltage in short circuit. Then from this base measurement, n set points are calculated based on the resolution selected to obtain the curve. Next with a PI control, this set points of current are followed by the system, and then the voltage is measured to obtain the pair of points to obtain the VI curve. Then the information is sent via serial and this information is shown in the program developed shown in Figure 19

3 Conclusions

During the development of this instrument, we established the importance of the model development and simulations results because even if the selected cell is not available at this moment, preliminary design can be done based on the simulation results. Also it is concluded that to estimate the solar

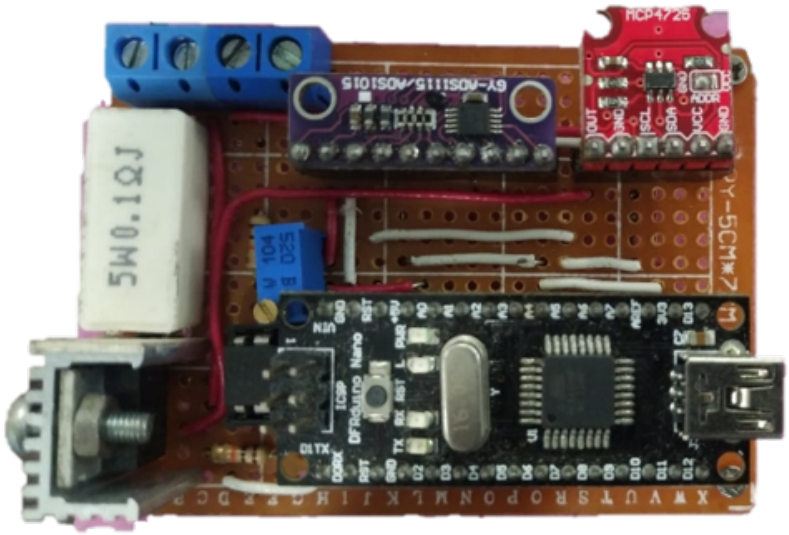

Figure 17: Circuit of the instrument

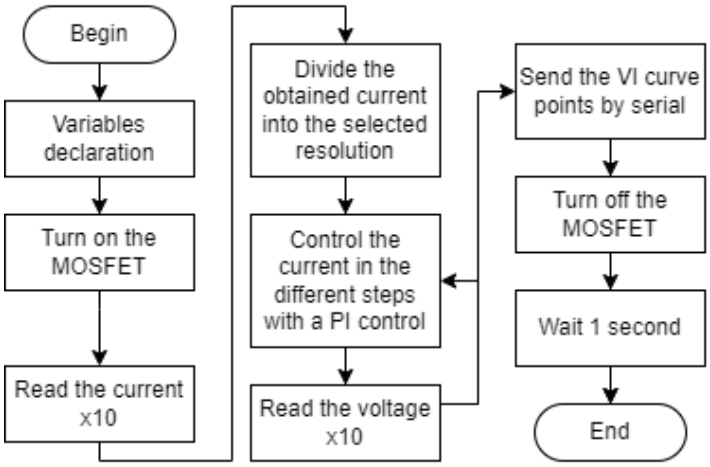

Figure 18: Flow chart for the software development

irradiation, is necessary to measure the short current and not the open voltage, because the voltage change in function of the solar irradiance doesn't change significantly and is very difficult to obtain trusted measurement due to the effect of the temperature. In this way calculating the solar irradiance from the area under the VI curve could improve the performance and the accuracy of the system. The temperature must be controlled or measured to improve the performance of the instrument because due to the effect of the leakage currents the measurement could change significantly in fuction of the

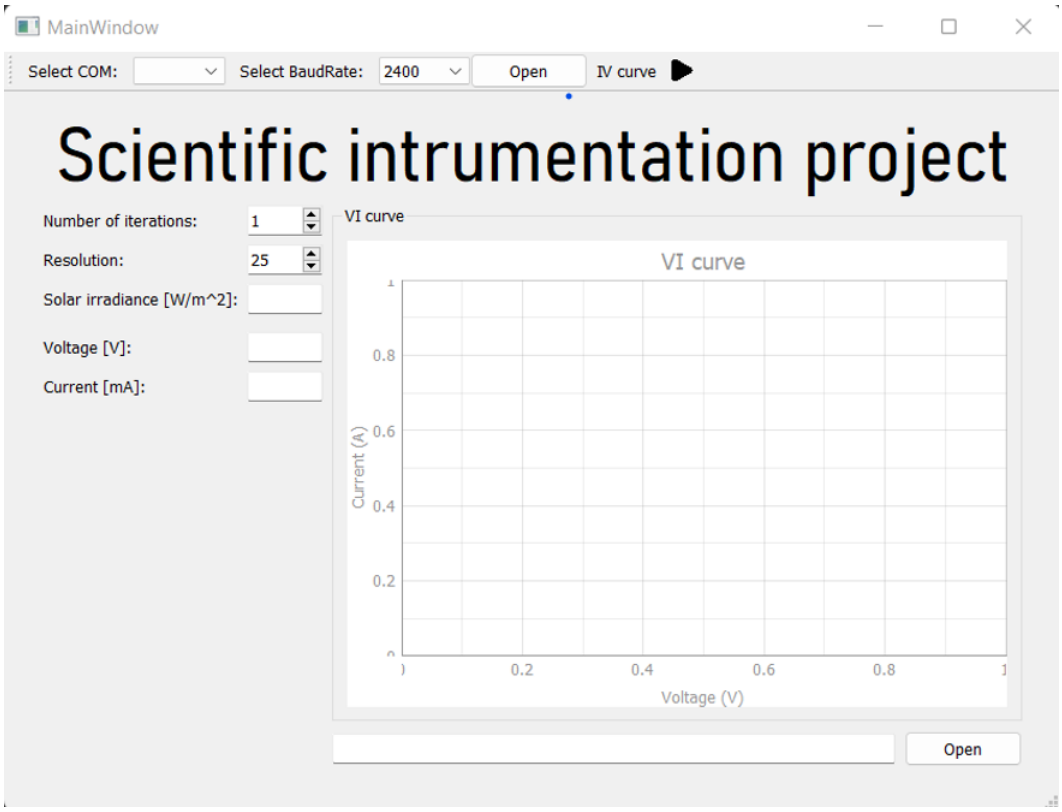

Figure 19: Flow chart for the software development

current. With a better cell its possible get better measurements. Finally with a xenon lamp is needed to calibrate the instrument accurately in different solar irradiations.

References

[1] Y. Karzazi and I. Arbouch, “Inorganic photovoltaic cells: Operating principles, technologies and efficiencies - review,” *Journal of Materials and Environmental Science*, vol. 5, pp. 1505–1515, 01 2014.

[2] X. Li, C. Zhang, Z. Yang, and A. Shang, “Broadband, polarization-insensitive and wideangle absorption enhancement of a-si:h/ìc-si:h tandem solar cells by nanopatterning a-si:h layer,” *Optics express*, vol. 21, pp. A677–A686, 07 2013.

[3] L. Solar, “Best Monocrystalline Solar Panels - Alternative Energy Sources,” https://alternativeenergysourcesv.com/best-monocrystalline-solar-panels/, apr 8 2018, [Online; accessed 2022-04-27].

[4] A. Adam, “Polycrystalline vs. Monocrystalline Solar Panels: Which Is Better?”

https://offgridtiny.house/polycrystalline-vs-monocrystalline-solar-panels-which-is-better/, dec 24 2017, [Online; accessed 2022-04-27].

[5] Mathworks, "Implement PV array modules - Simulink - MathWorks América Latina," https://la.mathworks.com/help/physmod/sps/powersys/ref/pvarray.html, [Online; accessed 2022-04-28].

[6] A. Hunt, "Amorphous vs crystalline solar panels: What's the difference?" https://solarsmarts.co/amorphous-vs-crystalline-solar-panels/, jul 21 2021, [Online; accessed 2022-04-27].

[7] A. M. Bagher, M. M. A. Vahid, and M. Mohsen, "Types of solar cells and application," *American Journal of optics and Photonics*, vol. 3, no. 5, pp. 94–113, 2015.

[8] W. Abd El-Basit, A. El–MAKSOOD, and F. Soliman, "Mathematical model for photovoltaic cells," *Leonardo Journal of Sciences*, vol. 12, pp. 13–28, 12 2013.